Ultrasound in Med. & Biol., Vol. 33, No. 6, pp. 941–949, 2007
Copyright © 2007 World Federation for Ultrasound in Medicine & Biology
Printed in the USA. All rights reserved
0301-5629/07/$–see front matter

ELSEVIER

doi:10.1016/j.ultrasmedbio.2006.11.004

● *Original Contribution*

THE ONSET OF MICROBUBBLE VIBRATION

MARCIA EMMER,*† ANNEMIEKE VAN WAMEL,*‡ DAVE E. GOERTZ,*‡ and NICO DE JONG*‡§
*Biomedical Engineering, Erasmus MC, Rotterdam, The Netherlands; †Stichting FOM, Utrecht, The Netherlands; ‡Interuniversity Cardiology Institute of the Netherlands, Utrecht, The Netherlands; §Physics of Fluids, University of Twente, Enschede, The Netherlands

(*Received* 14 *July* 2006, *revised* 24 *October* 2006, *in final form* 1 *November* 2006)

Abstract—A linear relationship between the relative expansion of an off-resonance ultrasound contrast microbubble and low acoustic pressures is expected. In this study, high-speed optical recordings of individual phospholipid-coated microbubbles were used to investigate this relationship for microbubbles ranging from 2 to 11 μm and for acoustic pressures ranging from 20 to 250 kPa at a driving frequency of 1.7 MHz. For microbubbles larger than 5 μm, the relative expansion ($\Delta D/D_0$) increased linearly with applied acoustic pressure, starting at the origin. The response of smaller microbubbles (<5 μm) also increased linearly with the applied acoustic pressure. However, linearity started at an acoustic pressure threshold value of 30 to 120 kPa for the different individual microbubbles. Below these pressure values, little or no oscillation was observed. The results may be explained by size-dependent mechanical properties of the phospholipid shells. An imaging technique such as power modulation imaging could profit from the presence of an acoustic pressure threshold in the microbubble response. (E-mail: m.emmer@erasmusmc.nl) **© 2007 World Federation for Ultrasound in Medicine & Biology.**

Key Words: **Ultrasound contrast agents, Microbubbles, Pressure-dependent threshold behavior, Optical observations.**

INTRODUCTION

Ultrasound (US) contrast agents consist of small (1 to 10 μm in diameter) encapsulated gas-filled microbubbles. In an ultrasound field, microbubbles oscillate due to the compressibility of their gas core. This oscillating behavior is the primary source of the high scattering strength of these agents, which makes them well suited to provide contrast enhancement in diagnostic US imaging.

Models like the RPNNP equation (Leighton 1994) are well established for gas microbubbles. However, although a number of models have been developed for encapsulated microbubbles, their ability to predict acoustic behavior has been shown to be valid only under limited circumstances. Further, the shell parameters required as input for these models have generally been achieved with bulk acoustic property measurements. In Gorce et al. (2000), for example, the shell is characterized by two parameters, the stiffness and the viscosity, using attenuation and scattering measurements from suspensions of microbubbles. As a result, such measurements may not be valid for predicting the behavior of each individual microbubble with its specific size and thickness, composition and packing of the phospholipid layer. Optical measurements also have been used to estimate shell properties, but under high amplitude (acoustic peak negative pressure >100 kPa) transmit conditions (Morgan et al. 2000).

Contemporary contrast imaging methods are based on exploiting differences between tissue echoes and the unique acoustical signatures of microbubbles (de Jong et al. 2002). For hard-shelled microbubbles, the principle of gas-release detection is used. The destruction mechanism of a hard-shelled polymer/albumin microbubble filled with nitrogen gas has been revealed by high-speed optical recordings (Bouakaz et al. 2005). When the applied acoustic pressure is higher than the threshold, the gas escapes from the shell and forms free gas bubbles. These gas bubbles produce distinct echo signals, which can be used to detect the contrast agent (Bouakaz et al. 2005; Frinking et al. 2001; Sboros et al. 2002).

Other microbubble imaging methods are typically used for soft-shelled contrast agents, which are more compliant than hard-shelled contrast agents. Soft-shelled microbubbles also fragment at high acoustic pressures

Address correspondence to: Marcia Emmer, MSc, Room Ee2302, Department of Biomedical Engineering, Thoraxcenter, Erasmus MC, P.O. Box 2040, 3000 CA Rotterdam, The Netherlands. E-mail: m.emmer@erasmusmc.nl

(Chomas et al. 2001; Postema et al. 2004), but, unlike hard-shelled microbubbles, they are already strong US scatterers at lower acoustic pressures. Multipulse detection methods at low mechanical index (Deng and Lizzi 2002; Eckersley et al. 2005) use the difference between the signatures of tissue and these microbubbles by preferentially detecting the nonlinear microbubble echoes and by canceling the background tissue signals.

Although encapsulated microbubbles are believed to respond differently under different driving-pressure amplitudes, few studies have been performed to study the pressure-dependence of their response in detail. Studies on the acoustic response have demonstrated that the pressure amplitude of the first harmonic is proportional to the incident peak pressure, whereas the second harmonic and third harmonic amplitudes are shown to be proportional to the square and cube of the incident peak pressure, respectively (Church 1995; Shi et al. 1999). Furthermore, the attenuation by encapsulated microbubbles in US propagation appeared to be dependent on the acoustic pressure (Chen et al. 2002; Tang et al. 2005). Optical studies have found that maximal bubble expansion increases for larger microbubbles (Postema et al. 2003).

In this study, we investigated the onset of phospholipid-coated microbubble vibration. For encapsulated microbubbles, the well-known Blake model does not apply (Leighton 1994). It is generally believed that in the small oscillation amplitude limit, an encapsulated microbubble behaves as a forced linear oscillator. This hypothesis implies that any input acoustic pressure on a resting microbubble results in a vibration, which increases proportional to an increasing acoustic pressure; however, this effect has never been investigated. High-speed optical recordings of individual microbubbles for specific resting microbubble sizes revealed a nonlinear relationship between radial excursion and low acoustic driving pressure. In this study, the results were compared with the outcome of theoretical descriptions and discussed in detail.

MATERIALS AND METHODS

Theory

The onset of microbubble vibration was investigated using the model by Church (1995) for encapsulated microbubbles. The model concerns air microbubbles enclosed in a solid, incompressible viscoelastic shell, which is described by a shear modulus G_S and a shear viscosity μ_S. It is assumed that the shell reduces the surface tension both at the shell-liquid and the shell-gas interfaces. As a result, the surface tension can be neglected. The shells of the investigated microbubbles consist of a lipid monolayer, which has a thickness of approximately 3 nm (Kim et al. 2003). We therefore assume a thin shell (Hoff et al. 2000), which results in the following equation of motion:

$$\rho_L\left(R\ddot{R}+\frac{3}{2}\dot{R}^2\right)=\rho_0\left(\frac{R_0}{R}\right)^{3\kappa}-\frac{4\mu_L\dot{R}}{R}-p_0-P_{ac}(t)-12\mu_S\frac{h_{S,0}R_0^{\,2}}{R^3}\frac{\dot{R}}{R}-12G_S\frac{h_{S,0}R_0^{\,2}}{R^3}\left(1-\frac{R_0}{R}\right) \quad (1)$$

where R is the microbubble radius, ρ_L is the density of the surrounding liquid (*i.e.*, water), R_0 is the radius at equilibrium, p_0 is the hydrostatic liquid pressure outside the microbubble, $P_{ac}(t)$ is the acoustic pressure, $h_{S,0}$ is the shell thickness, and the dots denote differentiation with respect to time. For the shell parameters, G_S 60 MPa and for μ_S 1.2 Ns/m^2 were taken, values compatible with those estimated experimentally for SonoVue™ in Gorce et al. (2000). Solving Equation 1 results in the radius or diameter of the microbubble as a function of time as a response on the applied acoustic pressure.

To study the microbubble excursion as a function of acoustic pressure, the diameter-time curves (*D-T* curves) of an encapsulated microbubble 3.0 μm in diameter were calculated. For comparison, the diameter-time curves of a 3.0 μm free gas microbubble also were calculated using the RPNNP equation (Leighton 1994). Bursts of 50 cycles with a peak pressure ranging from 0.1 to 100 kPa were applied at a center frequency of 1.7 MHz. After the transient response, $D_{max} - D_{min}$ (ΔD) normalized to the resting diameter (D_0) was determined as a function of the applied driving pressure $P_{ac}(t)$.

The equations of motion are highly nonlinear, as one would expect from a system where expansion cannot be symmetric with compression except at low driving pressures. Therefore ΔD was chosen to express microbubble excursion instead of D_{max} or D_{min}. To compare the linearity of the *D-T* curves between theoretical predictions and experimental results, the same parameters used in the previous calculation were applied to calculate the responses of 1- to 9 μm in diameter encapsulated microbubbles on 50 cycle-bursts with a frequency of 1.7 MHz and a peak pressure of 220 kPa. From the resulting *D-T* curves, the ratio between microbubble expansion E and compression C was determined, which was expressed by $E/C = |(D_{max} - D_0)/(D_{min} - D_0)|$.

Experiment

The experimental phospholipid-coated contrast agent used was BR14 (Bracco Research SA, Geneva, Switzerland). The microbubbles were injected into a cellulose Cuprophan® capillary tube (Akzo Nobel Faser AG, Germany) 160 μm in inner diameter and 200 μm in outer diameter, which is smaller than the acoustic wave-

length. Hydrophone measurements were performed to verify its acoustic transparency.

The capillary tube was placed in a water tank in the focal area of the transducer at 7.5 cm. The water tank was positioned under a customized BXFM microscope (Olympus Nederland B.V., Zoeterwoude, The Netherlands) with 2× U-CA magnification and a LUMPlanFl 100× water immersion objective lens (Olympus). No reflections from the objective were observed. Under the capillary tube, an optic fiber (Olympus) was mounted and was connected with the illumination source, which was an MVS-7010 Fiber Optic Strobe (PerkinElmer Optoelectronics, Salem, MA, USA). Images of individual microbubbles were recorded with the Brandaris 128 fast-framing camera system (Chin et al. 2003).

A v397-SU 2.25-MHz single element transducer (Panametrics Inc., Waltham, MA, USA) was mounted in the water tank at an angle of 45° relative to the top of the tank. Its aperture was 35 mm and the beam −6 dB in diameter at focus was 5 mm. The transducer was connected to an arbitrary waveform generator (Tabor Electronics Ltd., Tel Hanan, Israel) and a 60 dB linear power amplifier (AR Worldwide, Souderton, PA, USA). The amplitude was adjusted with two variable attenuators (Agilent Technologies, Inc., Palo Alto, CA, USA).

The pressure values were calibrated using a 0.2-mm PVDF needle hydrophone (Precision Acoustics Ltd., Dorchester, UK). For the transducer, previous studies have verified that the acoustic pressure was constant over a 200 μm distance in both axial and transversal directions, which corresponded to the capillary tube diameter (Bouakaz et al. 2005).

Individual microbubbles were recorded in 12 sequences of 64 image frames at a speed of 13 million frames per second, corresponding to 12 × 5 μs optical scanning duration. The time between the sequences was 50 ms. In each sequence, a single microbubble was insonified with a gated six-cycle-sine wave burst at 1.7 MHz center frequency, giving a US exposure time of 3.5 μs. The remaining 1.5 μs was used to record the microbubbles before US exposure, so that the resting microbubble size could be determined. The peak negative pressure was increased in subsequent sequences from 20 to 250 kPa. In a second experiment, we insonified single microbubbles with a Gaussian apodised burst with FWHM duration of 3.0 μs, a peak pressure of 250 kPa and a center frequency of 1.7 MHz.

Single microbubbles that were in the focus of the microscope (Postema et al. 2003) were selected. The diameters of the individual microbubbles were measured in each image frame with a semiautomatic procedure using a minimal cost algorithm in custom software, written in a Matlab environment (Mathworks Inc, Natick, MA, USA) resulting in the microbubble diameter response as a function of time. To increase the accuracy of the determination of the minima and maxima, the *D-T* data were interpolated at 20 times the original frame rate and filtered with a lowpass finite impulse response (FIR) filter. As a measure of the microbubble response, the difference between the maximum diameter and the minimum diameter, $D_{max} - D_{min}$ (ΔD) normalized to the resting diameter (D_0), was taken.

The relationship between $\Delta D/D_0$ and the acoustic driving pressure, $P_{ac}(t)$, was investigated. For this purpose, the linearity of the $\Delta D/D_0$ vs. P_{ac} curves was established by fitting least-squares trend lines through the linear portions of $\Delta D/D_0$ vs. P_{ac} and determining the intercepts with the pressure axis. The significance of the linear regression was investigated by calculating the square of the correlation coefficient, R^2, between the acoustic pressure and $\Delta D/D_0$ and determining the hypothesis that the slope of the trend line is zero. Only ΔD larger than the resolution limit of our system and responses smaller than 30% of the initial size, $\Delta D/D_0 < 0.3$, were used, because then it was assumed that the response was linear. The trend lines were based on at least three sample points.

To compare the experimentally obtained *D-T* curves with the outcome of the simulations and from the measured *D-T* responses, the *E/C* values were determined at an acoustic driving pressure of 220 kPa. The application of a Gaussian apodised burst was used to illustrate the shape of the *D-T* curve at the onset of microbubble oscillation.

Chin et al. (2003) have shown that at 120× magnification, the Brandaris 128 high-speed camera system resolves lines with 0.4 μm spacing. For this study, the stochastic error in the microbubble diameter measurements had to be established, because it determines the resolution limit of microbubble vibration. The stochastic error depends on a combination of the point-spread function of the optical system including the CCD grid, the CCD electronics and the minimum-cost algorithm used to measure the stochastic error. For our system, the stochastic error was established by determining the maximum diameter variation, ΔD, for each microbubble in the first sequence of image frames (*i.e.*, when no US was applied). Subsequently, the maximum ΔD for the whole population was determined, and this value was used as the resolution limit of microbubble vibration.

RESULTS

Theory

Both the free gas microbubble and the encapsulated microbubble 3.0 μm in diameter were driven at 1.7 MHz. This is below resonance for both cases, because the linear resonance diameter for a free gas microbubble is

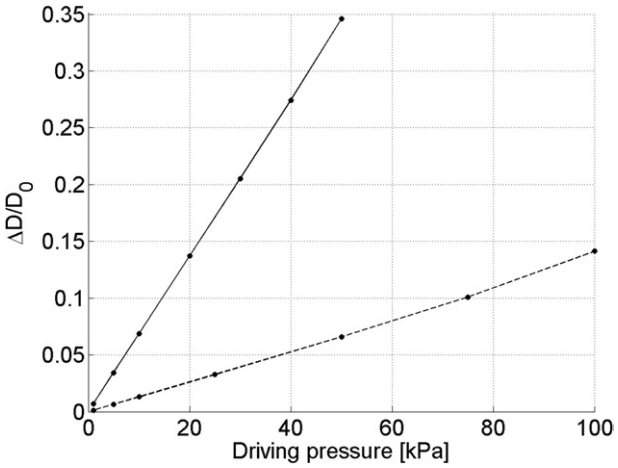

Fig. 1. Simulations of the responses of a 3.0 μm gas microbubble (solid line) and an encapsulated microbubble (dashed line) on different US driving pressures.

3.7 μm in diameter and an encapsulated microbubble is 6.2 μm in diameter. At low driving pressures, Fig. 1 shows that for both the free and the encapsulated microbubble, the amplitudes of oscillation increase linearly with the applied acoustic pressure. Figure 1 also makes clear that this linear relationship starts at the origin.

The numerical solutions gave highly nonlinear free microbubble oscillation motions above 50 kPa. For higher pressures, ΔD was demonstrated to not be a good measure of free microbubble oscillation. Also, for the encapsulated microbubble, acoustic pressures above 100 kPa resulted in a nonlinear response. As an example, Fig. 2a shows the *D-T* curve of an encapsulated microbubble 3.0 μm in diameter at a driving pressure of 220 kPa. The expansion amplitude ($D_{max} - D_0 = 1.0$ μm) is higher than the compression amplitude ($D_0 - D_{min} = 0.56$ μm), resulting in an *E/C* value of 1.8. Figure 2b shows the *E/C* values of encapsulated microbubbles ranging from 1 to 9 μm in diameter. The *E/C* values vary with microbubble size from 1.1 to 2.3, which shows that the expansion phases dominated the compression phases.

Experiment

To investigate the onset of microbubble oscillation, the results of 48 single microbubbles were analyzed. The smallest microbubble was 1.3 μm in diameter and the largest microbubble was 10.6 μm in diameter. The majority of the microbubbles (73%) was smaller than 4.0 μm in diameter.

First, the resolution limit of microbubble vibration was determined. For all measurements, the diameter variation when no US was applied was in the range of 66 to 150 nm with a mean of 100 nm and a standard deviation of 23 nm. One pixel in the image frame is 100 nm, and so the variation is approximately one pixel. The worst case (diameter variation of 150 nm) was taken as the resolution limit of microbubble vibration.

Figure 3a shows image frames of a 4.2 μm–diameter microbubble, which was insonified with an acoustic pressure of 250 kPa. The resulting *D-T* curve is shown in Fig. 3b. In the first 13 frames, the microbubble is at rest. Starting at frame 14, the microbubble is first compressed, and then reaches its maximum and minimum diameter of 5.4 and 2.6 μm, respectively, within six cycles.

The *D-T* curves for the complete range of applied acoustic pressures are shown in Fig. 4, which also includes the responses of three additional microbubbles of different sizes. The *D-T* curves demonstrate a relationship between resting diameter and the response. Larger microbubbles expand and compress more than smaller microbubbles, as was demonstrated in previous studies (Postema et al. 2003).

We noticed that the acoustic pressure at which the first microbubble vibration could be observed, decreased

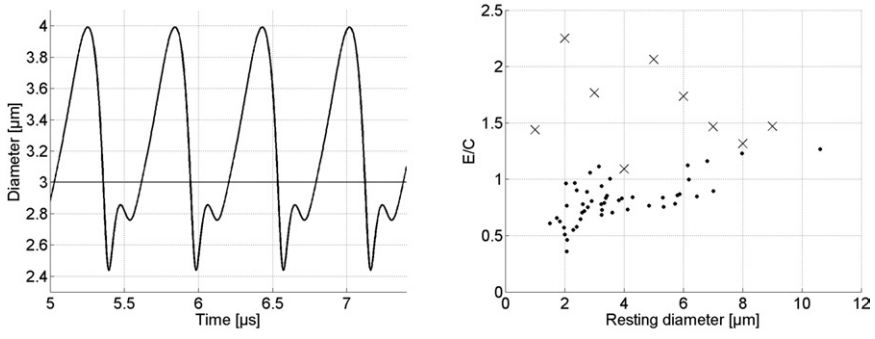

Fig. 2. (a) Simulated diameter-time response of a 3.0 μm encapsulated microbubble. (b) *E/C* values as a function of microbubble resting diameter of simulated encapsulated microbubble responses (x's) and measured encapsulated microbubble responses (dots), with $E/C = |(D_{max} - D_0)/(D_{min} - D_0)|$.

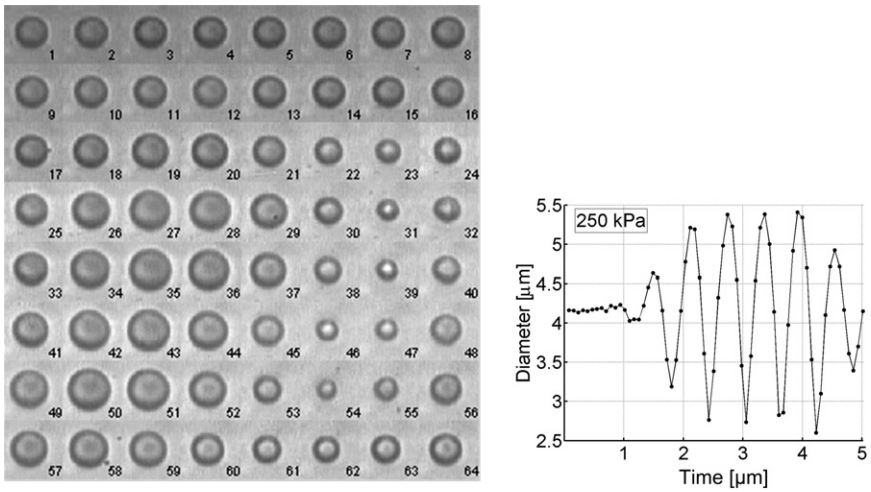

Fig. 3. (a) Sequence of 64 image frames of a 4.2 μm diameter microbubble, driven by a 6-cycle–US burst with a peak negative pressure of 250 kPa. (b) Diameter-time response.

with resting diameter. Furthermore, it was interesting to compare the responses of the two largest microbubbles. The maximal difference between maximal and minimal diameter (ΔD) for the microbubble 7.0 μm in diameter was 2.6 μm, which results in $\Delta D/D_0 \approx 0.4$. This is less than $\Delta D/D_0 \approx 0.7$ for the microbubble 4.2 μm in diameter. However, the first oscillations of the 7.0 μm microbubble were observed when the driving pressure was at its lowest value of 20 kPa, which differed from the observed response of the smaller microbubble. In that case, oscillations were not detected until the driving pressure was increased to 60 kPa. Although the microbubble 4.2 μm in diameter showed a stronger response, a higher acoustic driving pressure was needed to initiate oscillations.

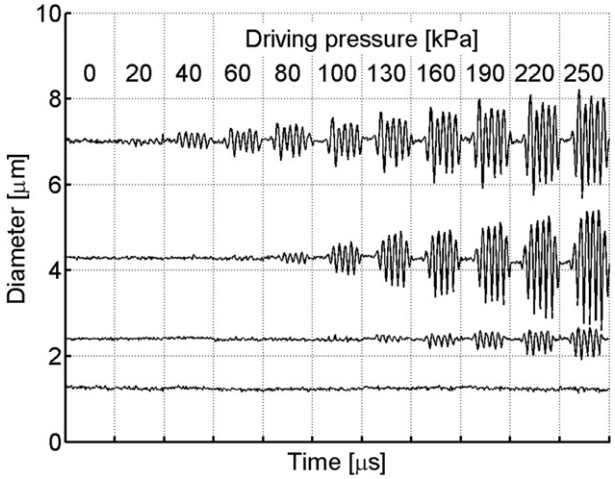

Fig. 4. Diameter-time responses of four microbubbles with a resting diameter of 1.3, 2.4, 4.2 and 7.0 μm. Vertical grid lines separate the sequences, and the applied driving pressure is indicated.

The microbubble excursion ($\Delta D/D_0$) as a function of the driving pressure $P_{ac}(t)$ was investigated for the complete data set of 48 microbubbles (Fig. 5). The microbubbles were categorized according to their resting diameters. Two microbubbles with diameters of 1.3 and 2.0 μm had no detectable oscillations. The responses showed a relationship between microbubble excursion and the applied acoustic driving pressure. In most cases, a higher acoustic pressure resulted in an increased excursion. For some microbubble sizes, however, this did not hold for the lowest applied acoustic pressures. For microbubbles smaller than 5 μm in diameter, the $\Delta D/D_0$ vs. P_{ac} curves did not start to rise at the origin, but at higher acoustic pressures.

The $\Delta D/D_0$ vs. P_{ac} curves of 38 microbubbles answered to the conditions posed for trend line fitting. Eleven lines were based on three measurements of $\Delta D/D_0$ vs. P_{ac}, 14 were based on four measurements and 13 on more than four measurements. The average of the R^2 values of these trend lines was 0.98 with a standard deviation of 0.025. Testing the significance of the trend line slopes resulted in an average p-value of 0.03 with a standard deviation of 0.05; 80% of these p-values was lower than 0.025.

From these trend lines the pressure axis intercepts were determined (Fig. 6). Microbubbles ranging from 2.0 to 4.0 μm had a pressure axis intercept between 30 and 120 kPa. Microbubbles larger than 5.0 μm had a pressure axis intercept approximating 0 kPa, ranging from -7 kPa

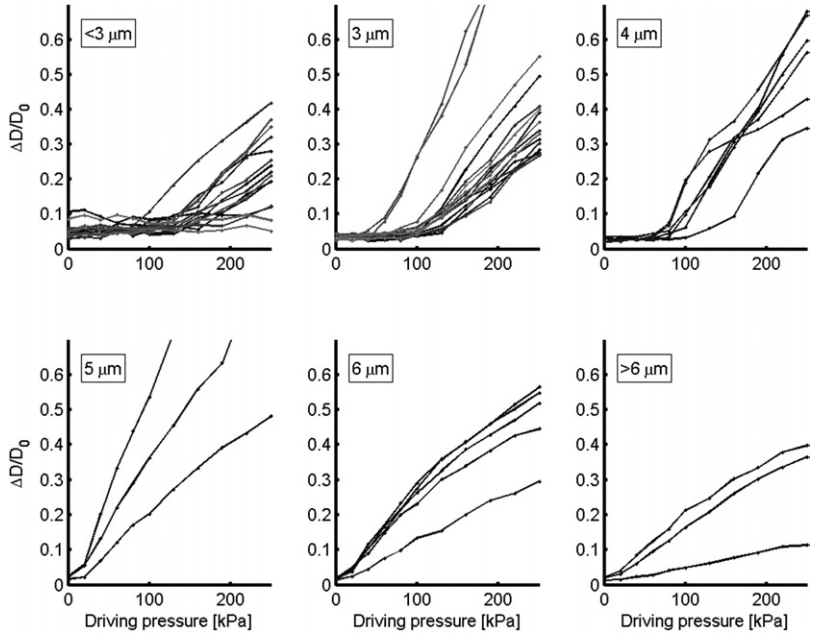

Fig. 5. Microbubble excursions as a function of acoustic pressure. The responses of the different microbubbles have been categorized according to their sizes, as indicated.

to 7 kPa. In addition, the linearity of the *D-T* curves was measured at an acoustic pressure of 220 kPa. Figure 2b shows that the *E/C* values of the measurements were between 0.4 and 1.25.

The onset of microbubble vibration was illustrated by the application of a Gaussian apodised burst. The *D-T* curves of three microbubbles that were 1.5, 2.1 and 7.7 μm in diameter, respectively, are shown in Fig. 7. After a transient time of approximately one cycle, the 7.7-μm microbubble responded with a phase shift of approximately half a cycle, which indicated that it was excited above resonance. The smaller microbubbles responded in phase with the applied US field, but they required a higher acoustic driving pressure before their oscillations became apparent, an observation consistent with the observations demonstrated in Figs. 4 and 5. The shape of these *D-T* curves also was notable. The response of the

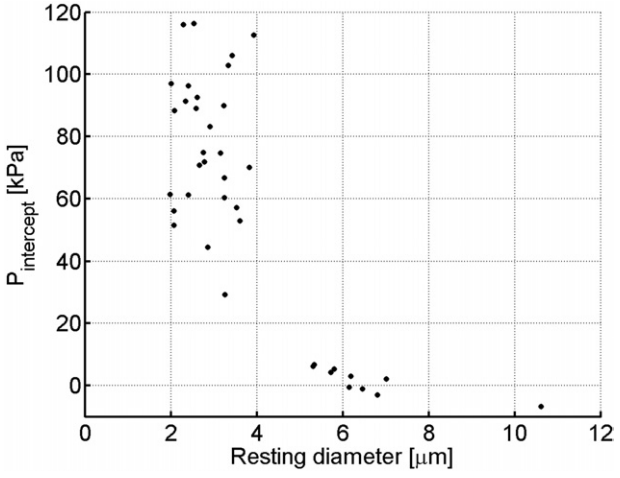

Fig. 6. The intercepts with the pressure axis of the linear part of the microbubble responses as a function of resting diameter.

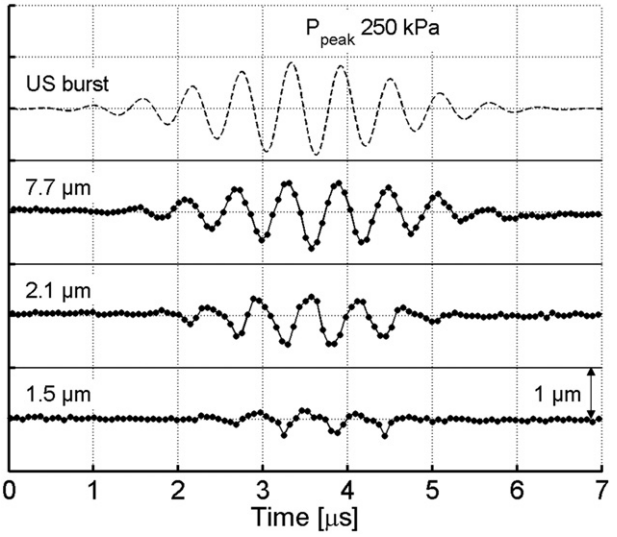

Fig. 7. *D-T* curves of microbubbles with a resting diameter of 1.5 μm, 2.1 μm and 7.7 μm. The horizontal grid lines represent 1 μm. The dashed line (US burst) shows the applied Gaussian apodised US burst with a peak pressure of 250 kPa.

7.7-μm microbubble had a nearly symmetrical shape: expansion approximates compression ($E/C = 0.8$). The microbubble that was 2.1 μm in diameter had an E/C of 0.7. However, the D-T curve of the 1.5-μm in diameter microbubble was highly nonlinear. Approximately six frames cover the expansion phase of the microbubble, and only three frames cover the compression phase of the microbubble. At a frame rate of 13 million frames per second, the expansion phase was 0.46 μs, and the compression phase was 0.23 μs. In less time, the negative amplitude ($D_0 - D_{min}$) was maximal 0.3 μm and the positive amplitude ($D_{max} - D_0$) was maximal 0.15 μm, which resulted in an E/C value of 0.5. This microbubble was more compressed than expanded. Furthermore, the shape of the compression phase was much sharper than is generally expected in sinusoidal responses.

Discussion and conclusions

The theory predicted, for both a free and encapsulated microbubble that were 3.0 μm in diameter, a linear response for acoustic pressures below 50 and 100 kPa, respectively (Fig. 1). However, measured responses of microbubbles that were 3.0 μm in diameter showed clearly different behaviors (Fig. 5). The acoustic pressure needed to increase above a threshold value before the microbubble responses increased linearly with the applied acoustic pressure. Trend lines were fitted through the linear portions of the $\Delta D/D_0$ vs. P_{ac} curves. Although statistics on these trend lines was limited by the low number of available sample points for each fit, we concluded that the lines could be used to determine the pressure axis intercepts and so obtain estimations of the threshold values of the onset of linear oscillation as a function of acoustic pressure. From Figs. 5 and 6, it appears that microbubbles with a resting diameter smaller than 5 μm show threshold behavior, and larger microbubbles do not show this behavior.

Because the observation of the microbubble response was limited by the system resolution of 150 nm, it is not known if the microbubbles oscillated at acoustic pressures below the acoustic pressure threshold. Furthermore, microbubbles larger than 5 μm may also have an acoustic pressure threshold lower than 20 kPa, but this was not investigated. We did notice that the threshold values did not show a clear relationship with resting diameter, which might be due to differences in composition of the encapsulated microbubbles, and, in some cases, to the low number of sample points. However, in contrast to theoretical predictions, we have demonstrated (for encapsulated microbubbles smaller than 5 μm) that, at the onset of microbubble vibration, the response as a function of acoustic pressure was nonlinear and that an acoustic pressure threshold indicated the transition into

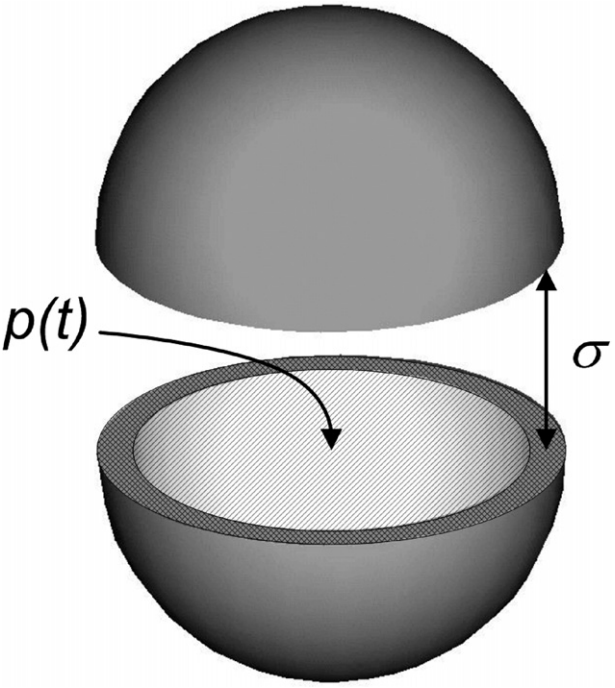

Fig. 8. In a simplified perception of microbubble expansion, the microbubble is a globe with two hemispheres that need to separate at the equator. The acoustic pressure $p(t)$ acts on the cross-section of the microbubble πR^2, as the tensile strength σ acts on the shell area $2\pi Rh$.

responses, which increased proportionally to the acoustic pressure applied.

In addition to the observed threshold behavior, we found a second indication that current models do not fully describe encapsulated microbubble behavior—the difference in the shape of the microbubble response itself. Figure 2b illustrates that, at an acoustic pressure of 220 kPa, measured E/C values differed greatly from predicted values. When simulations predicted dominant expansion ($E/C > 1$), measured values showed more compression up to symmetrical shapes ($E/C > 1$).

The pressure threshold for microbubble oscillation is a new observation, and the precise mechanism is not currently known. One explanation is that a force threshold must be overcome before substantial oscillations can occur. For simplicity, it has been assumed that microbubble oscillation contains an expansion phase. The microbubble is considered to be a sphere comprised of two hemispheres that need to separate at the equator (see Fig. 8). We then assume that the microbubble can only expand in the negative phase of insonation when the shell breaks along the interface between the two hemispheres. The force required to overcome the tensile strength (σ) of the phospholipid shell is $\sigma \cdot 2\pi R \cdot h$. The force made available by the insonating field to overcome this force is $p(t) \cdot \pi R^2$. Therefore, an estimate of the acoustic pressure

Table 1. Shape of the *D-T* curve at the onset of microbubble vibration, classified as E/C ≥ 0.5 ("compression-only") or E/C > 0.5 ("symmetrical").

Microbubble size (μm)	1–1.9	2–2.9	3–3.9	4–4.9	5–5.9	6–6.9	>7
Compression only, n (%)	2 (100)	10 (59)	3 (25)	0 (0)	0 (0)	0 (0)	0 (0)
Total observed, n	2	17	12	2	6	4	3

required to split the two hemispheres is $p = \sigma 2\pi Rh/\pi R^2 = 2\sigma h/R$. From this relation, it appears that the acoustic pressure threshold is inversely proportional to the microbubble radius, and so relatively more force is necessary for the vibration of small microbubbles.

The value of the tensile strength of the phospholipid monolayer is not known. We therefore assume a value of 10 MPa, which is the tensile strength of polyethylene (Nakamura et al. 2005). For a microbubble of 1.0 μm in diameter and a shell thickness of 3 nm, we found that the acoustic pressure threshold *p(t)* for the onset of microbubble vibration is 60 kPa. This is in the same order of magnitude as the experimentally obtained threshold values.

In reality, it is unlikely that the microbubble cracks into two perfect hemispheres, as it is unlikely that the coatings are completely homogeneous. Borden et al. (2004) have found that microbubbles may form domains that are in the condensed phase separated by boundaries, which are in the expanded phase. The size and distribution of the domains depend on the types of lipids used and the processing conditions and influence microstructure and mechanical properties of the microbubbles (Kim et al. 2003). Also shrinkage may lead to differences between the mechanical properties of shells. Any finite interfacial tension leads to a Laplace pressure that drives gas out of the microbubble even in saturated solution (Duncan and Needham 2004). As the gas leaves, compression of the monolayer shell leads to tight packing of the condensed phase (Kim et al. 2003). As a consequence of the described influences, smaller microbubbles may have a higher tensile strength than larger microbubbles, which increases their acoustic pressure threshold for the onset of microbubble vibration.

Another indication for the influence of the phospholipid packing on microbubble behavior is the observation of asymmetric diameter response curves, which has earlier been described as "compression-only" behavior (Marmottant et al. 2005) and is defined as $E/C < 0.5$ (de Jong et al. 2007). The high Van der Waals forces in the tightly packed monolayer inhibit both expansion and compression of the microbubble. However, when the pressure is increased enough, the monolayer can fracture and break, lose material or buckle and fold (Lipp et al. 1998). In the latter case, the microbubble is more easily compressed, which explains the dominant negative radial excursions. We observed "compression-only" behavior in the responses obtained after applying the Gaussian apodised burst (Fig. 7), but it was also noticed when the US bursts with constant amplitude were used (Fig. 2b). Figure 2b demonstrates that "compression-only" behavior, like threshold behavior, may be related to resting microbubble size. Moreover, it was especially noticed at the onset of microbubble vibration. In addition, the *D-T* curve shapes were determined during the first microbubble vibrations that were observed. The *E/C* values were classified as $E/C \leq 0.5$ ("compression-only") or $E/C > 0.5$ ("symmetrical") (Table 1). Table 1 also shows that "compression-only" behavior may be dependent on size; only microbubbles smaller than 4 μm showed this typical asymmetric radial shape, whereas microbubbles larger than 4 μm started oscillating in a (more) symmetrical form.

Another influence on microbubble behavior may be the capillary tube in which the microbubbles were inserted. Buoyancy drives the microbubbles toward the tube wall. Previous studies have shown, for example, a constrained microbubble activity in a tube 12 μm in diameter (Caskey et al. 2005), and asymmetric oscillations of a targeted microbubble (Zhao et al. 2005). The influence of the presence of a rigid wall on the onset of microbubble vibration, however, has yet to be established.

The presence of an acoustic pressure threshold will have implications for the acoustic microbubble responses. For a linear system, the attenuation by the microbubbles in US propagation is independent of the insonifying acoustic pressure. However, previous studies (Tang et al. 2005) have shown a linear relationship between the attenuation of phospholipid microbubbles and the insonating acoustic pressure for acoustic pressures down to 20 kPa. The presence of an acoustic pressure threshold may explain these results. Below this threshold, only the largest microbubbles oscillate significantly and contribute to the attenuation. As the acoustic pressure is increased, the smaller microbubbles also will contribute and increase the attenuation.

The results of our study reveal the complex nature of the onset of phospholipid contrast agent vibration. For microbubbles smaller than 5 μm in diameter, the acoustic pressure needed to increase above 30 to 120 kPa before their responses increased linearly with the applied

acoustic pressure. Possible explanations are size-dependent mechanical properties of the phospholipid shells. More research will lead to a better understanding of microbubble oscillation, which could be exploited to enhance the contrast between tissue and microbubbles in imaging techniques. A technique such as power modulation imaging (Deng and Lizzi 2002) could especially profit from the presence of such a pressure offset in the microbubble response. However, further research is needed to fully use these specific characteristics of microbubble behavior.

Acknowledgements—The authors thank Alexander Klibanov (University of Virginia) and Marcel Böhmer (Philips Research) for their interest and fruitful discussions. This work is part of the research programme of the 'Stichting voor Fundamenteel Onderzoek der Materie (FOM)', which is financially supported by the 'Nederlandse Organisatie voor Wetenschappelijk Onderzoek (NWO)'. We acknowledge Bracco Research, Geneva, for supplying the contrast agent BR14.

REFERENCES

Borden MA, Pu G, Runner GJ, Longo ML. Surface phase behavior and microstructure of lipid/PEG-emulsifier monolayer-coated microbubbles. Colloids and Surfaces 2004;35:209–223.

Bouakaz A, Versluis M, de Jong N. High-speed optical observations of contrast agent destruction. Ultrasound Med Biol 2005;31:391–399.

Caskey C, Kruse D, Dayton P, Ferrara K. On the oscillations of microbubbles in tubes with diameters as small as 12 microns. Proc IEEE Ultrason Symp 2005;854–857.

Chen Q, Zagzebski J, Wilson T, Stiles T. Pressure-dependent attenuation in ultrasound contrast agents. Ultrasound Med Biol 2002;28: 1041–1051.

Chin CT, Lancée C, Borsboom J, et al. Brandaris 128: A 25 million frames per second digital camera with 128 highly sensitive frames. Rev Sci Instru 2003;74:5026–5034.

Chomas JE, Dayton P, May D, Ferrara K. Threshold of fragmentation for ultrasonic contrast agents. J Biomed Opt 2001;6:141–150.

Church CC. The effects of an elastic solid surface layer on the radial pulsations of gas bubbles. J Acoust Soc Am 1995;97:1510–1521.

de Jong N, Bouakaz A, ten Cate FJ. Contrast harmonic imaging. Ultrasonics 2002;40:567–573.

de Jong N, Emmer M, Chin CT, et al. "Compression-only" behavior of phopholipid-coated contrast bubbles. Ultrasound Med Biol 2007; 33:653–656.

Deng CX, Lizzi FL. A review of physical phenomena associated with ultrasonic contrast agents and illustrative clinical applications. Ultrasound Med Biol 2002;28:277–286.

Duncan PB, Needham D. Test of the Epstein-Plesset model for gas microparticle dissolution in aqueous media: Effect of surface tension and gas undersaturation in solution. Langmuir 2004;20:2567–2578.

Eckersley RJ, Chin CT, Burns PN. Optimising phase and amplitude modulation schemes for imaging microbubble contrast agents at low acoustic power. Ultrasound Med Biol 2005;31:213–219.

Frinking PJA, Cèspedes EI, Kirkhorn J, Torp HG, de Jong N. A new ultrasound contrast imaging approach based on the combination of multiple imaging pulses and a separate release burst. IEEE Trans Ultrason Ferroelect Freq Contr 2001;48:643–651.

Gorce J-M, Arditi M, Schneider M. Influence of bubble size distribution on the echogenicity of ultrasound contrast agents: A study of SonoVue. Invest Radiol 2000;35:661–671.

Hoff L, Sontum P, Hovem J. Oscillations of polymeric microbubbles: Effect of the encapsulating shell. J Acoust Soc Am 2000;107:2272–2280.

Kim DH, Costello MJ, Duncan PB, Needham D. Mechanical properties and microstructure of polycrystalline phospholipid monolayer shells: Novel solid microparticles. Langmuir 2003;19:8455–8466.

Leighton TG. The acoustic bubble. London: Academic Press Ltd., 1994.

Lipp MM, Lee KYC, Takamoto DY, Zusadzinski JA, Waring AJ. Coexistence of buckled and flat monolayers. Phys Rev Lett 1998; 81:1650–1653.

Marmottant P, Van der Meer S, Emmer M, et al. A model for large amplitude oscillations of coated bubbles accounting for buckling and rupture. J Acoust Soc Am 2005;118:3499–3505.

Morgan KE, Allen JS, Dayton PA, et al. Experimental and theoretical evaluation of microbubble behavior: Effect of transmitted phase and bubble size. IEEE Trans Ultrason Ferroelect Freq Contr 2000; 47:1494–1509.

Nakamura EM, Cordi L, Almeida GSG, Duran N, Mei LHI. Study and development of LDPE/starch partially biodegradable compounds. J Materials Processing Technology 2005;162–163:236–241.

Postema M, Bouakaz A, Chin CT, De Jong N. Simulations and measurements of optical images of insonified ultrasound contrast microbubbles. IEEE Trans Ultrason Ferroelect Freq Contr 2003;50: 523–536.

Postema M, van Wamel A, Lancee CT, de Jong N. Ultrasound-induced encapsulated microbubble phenomena. Ultrasound Med Biol 2004; 30:827–840.

Sboros V, MacDonald CA, Pye SD, et al. The dependence of ultrasound contrast agents backscatter on acoustic pressure: theory versus experiment. Ultrasonics 2002;40:579–583.

Shi WT, Forsberg F, Raichlen JS, Needleman L, Goldberg BB. Pressure dependence of subharmonic signals from contrast microbubbles. Ultrasound Med Biol 1999;25:275–283.

Tang MX, Eckersley RJ, Noble JA. Pressure-dependent attenuation with microbubbles at low mechanical index. Ultrasound Med Biol 2005;31:377–384.

Zhao S, Ferrara K, Dayton P. Asymmetric oscillation of adherent targeted ultrasound contrast agents. Appl Phys Lett 2005; 87:134103.